HHS Public Access

Author manuscript

Oncogene. Author manuscript; available in PMC 2022 July 08.

Published in final edited form as:

Oncogene. 2022 February ; 41(9): 1309–1323. doi:10.1038/s41388-021-02169-7.

Elevated expression of the colony-stimulating factor 1 (CSF1) induces prostatic intraepithelial neoplasia dependent of epithelial-Gp130.

Oh-Joon Kwon[1,#], **Boyu Zhang**[2,#], **Deyong Jia**[1], **Li Zhang**[1], **Xing Wei**[1], **Zhicheng Zhou**[1], **Deli Liu**[3], **Khoi Trung Huynh**[4], **Kai Zhang**[1], **Yiqun Zhang**[5], **Paul Labhart**[6], **Andrea Sboner**[3], **Chris Barbieri**[3], **Michael C Haffner**[7], **Chad J Creighton**[5], **Li Xin**[1,8,9]

[1:]Department of Urology, University of Washington, Seattle, WA 98109

[2:]Department of Molecular and Cellular Biology, Baylor College of Medicine, Houston TX 77030

[3:]Sandra and Edward Meyer Cancer Center and Department of Urology, Weill Cornell Medicine, New York, New York, USA

[4:]Department of Biology, University of Washington, Seattle, WA 98109

[5:]Dan L. Duncan Comprehensive Cancer Center, Baylor College of Medicine, Houston, TX 77030

[6:]Active Motif, San Diego, CA

[7:]Department of Laboratory Medicine and Pathology, University of Washington, Seattle, WA 98109

[8:]Institute of Stem Cell and Regenerative Medicine, University of Washington, Seattle, WA 98109

Abstract

Macrophages are increased in human benign prostatic hyperplasia and prostate cancer. We generate a *Pb-Csf1* mouse model with prostate-specific overexpression of macrophage colony-stimulating factor (*M-Csf*/*Csf1*). *Csf1* overexpression promotes immune cell infiltration into the prostate, modulates the macrophage polarity in a lobe-specific manner, and induces senescence and low-grade prostatic intraepithelial neoplasia (PIN). The *Pb-Csf1* prostate luminal cells exhibit increased stem cell features and epithelial-to-mesenchymal transition. Human prostate cancer

[9:]Corresponding author Li Xin, Ph.D., University of Washington, 850 Republican Street, Seattle, WA 98109, Phone: 206-543-6551, xin18@uw.edu.

[#:]These authors contributed equally.

Author Contributions

L.X., B.Z., and O.K. designed the experiments.
O.K., B.Z., L.Z., X.W., Z.Z., D.J., K.T.H., D. L. and K.Z. performed experiments.
O.K., B.Z., Y.Z., P.L., C.J.C., M.H., A. S., C. B., and L.X. analyzed the data.
L.X. wrote the manuscript with input from other authors.
O.K. and B.Z. contributed equally to the work.

Accession codes

RNA-Seq data have been deposited to GEO: GSA134326.

Conflict of Interest

The authors have no conflict of interest to declare.

patients with high *CSF-1* expression display similar transcriptional alterations with the *Pb-Csf1* model. *P53* knockout alleviates senescence but fails to progress PIN lesions. Ablating epithelial *Gp130* but not *Il1r1* substantially blocks PIN lesion formation. The androgen receptor (AR) is downregulated in *Pb-Csf1* mice. ChIP-Seq analysis reveals altered AR binding in 2482 genes although there is no significant widespread change in global AR transcriptional activity. Collectively, our study demonstrates that increased macrophage infiltration causes PIN formation but fails to transform prostate cells.

Keywords

prostate inflammation; colony-stimulating factor 1; senescence; Gp130; androgen receptor

Introduction

Inflammatory signaling plays a critical role in initiation and progression of various types of cancer including the prostate cancer (1, 2). Mutations and single-nucleotide polymorphisms in inflammation-related genes have been associated with prostate cancer risk (3). Epidemiological studies also showed that men with more inflammation in their baseline biopsies have a greater prostate cancer risk and that patients with inflammation in biopsy cores are more likely to develop advanced prostate cancer (4-6). Finally, histopathological analysis revealed frequent transitions between regions of prostatic atrophy associated with inflammatory cell infiltrates (proliferative inflammatory atrophy, PIA) and high grade prostatic intraepithelial neoplasia (PIN), leading to the hypothesis that PIAs could be the precursors of PIN lesions (7).

Inflammation contributes to prostate cancer initiation and progression via various mechanisms. Inflammation can enhance the accumulation of reactive oxygen species and promotes genetic and epigenetic alterations (8, 9). Inflammatory signaling can modulate androgen receptor signaling (10, 11) and alter immune response (12). Finally, inflammation can also regulate prostate epithelial differentiation program and increase the pool of the cell population that is sensitive to oncogenic transformation (13, 14). Genetic studies using mouse models demonstrated that activation of inflammatory signaling pathways such as NF-κB in the prostate epithelial cells can synergize with oncogenic signaling to promote progression of prostate cancer (15-17). However, whether prostate inflammation *per se* can transform prostate epithelial cells remains inconclusive. Mouse models of prostate inflammation induced by bacterial infection or autoimmunity have been established (18-20). The acute inflammation induced in these models often leads to severe damages in prostatic glandular structures and causes widespread compensatory epithelial proliferation and development of prostatic hyperplastic structures. However, most human prostate inflammation is asymptomatic. Some mouse models that simulate asymptomatic chronic prostate inflammation have also been generated such as those with prostate specific expression of the inflammatory growth factors and cytokines such as *Il1β*, *Il6*, and *Tgfβ* etc. (21-23). These models usually develop mild hyperplasic growth with a long latency. It remains unknown whether these inflammatory factors can cooperate or synergize

to transform prostate epithelial cells and whether specific inflammatory factors play a dominant role.

Macrophages and T cells are the major immune cells found in the prostate. Macrophages are often increased in human benign prostatic hyperplasia and prostate cancer (24, 25). Previously, we showed that macrophages are the major sources of many inflammatory cytokines such as Il1α/β etc. in the mouse prostate (26). Macrophage colony-stimulating factor (M-CSF/CSF1) plays a critical role in macrophage recruitment and survival as well as polarization of the cancer-related anti-inflammatory M2 phenotype of macrophage (27). It has been shown that ectopic expression of *Csf1* alone in the mouse mammary gland induced the formation of glandular dysplasia, ductal hyperplasia, and palpable mammary tumors (28). Based on these observations, we reason that ectopic expression of *Csf1* in mouse prostates should recruit macrophages and other types of immune cells, leading to an increased level of various cytokines and chemokines within the prostate. In this study, we generate a mouse model with prostate specific overexpression of *Csf1*, with which we study whether inflammatory signaling can cooperate to transform prostate epithelial cells and identify the most dominant inflammatory factors. Inflammatory signaling has been shown to alter AR signaling *in vitro* (11, 29) but it is less conclusive how the AR transcriptional activity is altered in the context of prostate inflammation *in vivo*. We also investigate how AR binding at a genome scale is affected using this new mouse model.

Results

Csf1 overexpression in mouse prostate induces immune cell infiltration.

We developed a transgenic mouse model with the rat probasin promoter driving the expression of the mouse *Csf1* transgene (hereafter referred to as the *Pb-Csf1* model) (Fig. 1A). The procedure for generating the *Pb-Csf1* model was described in detail in the Methods section. We screened offspring of 8 founders to determine whether the transgene was appropriately expressed in the prostate at both RNA (Supplementary Fig. 1A) and protein levels (Supplementary Fig. 1B) and whether transgene expression successfully induced infiltration of leukocytes into the prostate (Supplementary Fig. 1C). Two lines (#717 and #744) were selected for subsequent studies based on these criteria. The transgene is also expressed in epididymis or seminal vesicles but not in the other 11 major organs examined (Supplementary Fig. 1D). The data presented hereafter were obtained from the line #744, but all the phenotypes were confirmed in the other line unless stated otherwise.

Pb-Csf1 mice were born at the expected Mendelian ratio and exhibited normal behaviors and body weights relative to littermate controls at the age of 12 weeks, but they weighed slightly less than the control mice at the age of 1 year. The ratio of prostate versus body weight of *Pb-Csf1* mice was slightly reduced (WT: 0.0027 ± 0.00073 vs *Pb-Csf1*: 0.0023 ± 0.00055) (Supplementary Fig. 1E). QRT-PCR (Fig. 1B) analysis showed that *Csf1* was substantially expressed in the prostate tissues. ELISA analysis showed that Csf1 was expressed approximately 60-fold higher in the *Pb-Csf1* mice than control littermates (Fig. 1C). Flow cytometric analysis showed an approximately 2.65-fold increase in the $CD45^+$ leukocytes in the ventral prostate (VP) lobes of 1-year-old *Pb-Csf1* mice (WT: 6.66 ± 0.63% and *Pb-Csf1*: 17.7 ± 0.84%) (Fig. 1D), but the percentages of individual immune

cell lineages within the $CD45^+$ leukocytes remained comparable (Fig. 1E). The increased immune cell infiltration was less prominent in the anterior prostate (AP) (WT: 5.74 ± 0.26 %; *Pb-Csf1*: 6.70 ± 0.20 %) (Fig. 1D). This was probably because *Csf1* is expressed at a relatively lower level in AP (Supplementary Fig. 1A). Due to the high auto fluorescent background in the dorsolateral (DLP) lobes we were not able to quantify the leukocyte density. Of note, the average cell numbers in AP, DLP, and VP of the *Pb-csf1* mice increased by 8.60%, 42.0%, and 140% than those of the control mice, respectively. This indicates that the absolute numbers of all immune cells were increased in the *Pb-Csf1* model.

An RT^2 profiler PCR array for mouse cytokines and chemokines was used to determine whether infiltrated immune cells resulted in higher expression of cytokines and chemokines in the prostatic microenvironment. Supplementary Table 1 summarizes the results of PCR cytokine array. 52 out of 84 cytokines, chemokines and their corresponding receptors were upregulated by at least 1.5-fold in the *Pb-Csf1* mouse prostate tissues. The upregulation of some cytokines and chemokines including Il1α, Tnfα, Ccl2/5, and Cxcl1/2, etc. was also confirmed by a cytokine antibody array (Fig. 1F). In summary, prostate epithelial overexpression of Csf1 successfully induced immune cell infiltration and resulted in a microenvironment with upregulated cytokines and chemokines.

The macrophages polarize into a continuum ranging from the M1-like pro-inflammatory state to the anti-inflammatory M2-like state. We investigated whether exogenous Csf1 expression altered the polarity of prostatic macrophages by flow cytometric analysis of the surface markers for the M1 and M2 macrophages. Fig. 1G showed that the $F4/80^+CD11b^+$ macrophages in different prostatic lobes in wild type mice display distinct spectrums of polarization status. The ratios of the M1 ($MHCII^+CD206^{low}$) to M2 ($MHCII^+CD206^{high}$) macrophages in AP and VP of 1-yr-old WT mice were 1.35 and 3.09, respectively. In contrast, the corresponding ratios in the AP and VP of *Pb-Csf1* mice were 0.81 and 4.60, respectively. These results show that there is a slight shift of the macrophage polarity towards the M2 and M1 phenotypes in AP and VP, respectively, in the *Pb-Csf1* model. QRT-PCR analyses also confirmed that the M2 macrophage associated genes *Mrc1* and *Stat6* were upregulated in the FACS isolated macrophages in AP but downregulated in VP whereas the M1 associated genes *Nos2* and *Stat1* changed in the opposite manner (Fig. 1H). Not all markers associated with the M1 and M2 macrophages were altered accordingly (Supplementary Fig. 1F).

Csf1 overexpression induces prostatic intraepithelial neoplasia in ventral prostate.

The wild-type mouse prostate glands were composed of a single layer of luminal epithelial cells with eosinophilic secretions and pyknotic intraluminal cells suspended inside the glandular lumen at the age of 1 year (Fig. 2A). *Pb-Csf1* mice showed multifocal peri-glandular immune cell infiltrates (yellow arrows, Supplementary Fig. 2B), mostly in the ventral prostate (VP). The epithelial cells demonstrated mild to moderate nuclear atypia and focal multilayering in VP around 16 weeks of age, consistent with PIN II (30) (Supplementary Fig. 2A). PIN lesions developed focally and there was a vast heterogeneity in the percentage of area with PIN lesions in VP among experimental mice, ranging from 54.2% to 97.6% (N=9) (Fig. 2B) In addition, scattered luminal cell atrophy and basal cell

hyperplasia were noted. In contrast, very few atypical glands were noted in AP and DLP even in 1-year-old mice, although sporadic foci of immune cell infiltration were also noted (yellow arrows, Supplementary Fig. 2B). The *Pb-Csf1* mice did not develop PIN lesions in AP. Immunostaining of the basal cell markers (Krt5, Krt14 and Trp63) and luminal cell markers (Krt8 and Nkx3.1) and the androgen receptor (AR) showed that the PIN lesions composed of luminal cells surrounded by basal cells (Fig. 2C). The putative intermediate cells dual positive for both Krt5 and Krt8 were occasionally observed in the *Pb-Csf1* model (Fig. 2C). Masson trichrome staining showed enhanced extracellular matrix remodeling of collagen deposition in the prostate of 1-year-old *Pb-Csf1* mice (Fig. 2D). There is also an increased vascular density in the *Pb-Csf1* mice as shown by immunostaining of CD31 (Fig. 2E). Immunostaining for Ki67 showed that the proliferation index of epithelial cells in *Pb-Csf1* mice was 7-fold higher than that of age matched control mice (WT: 0.48 ± 0.18% and *Pb-Csf1*: 3.56 ± 0.57%) (Fig. 2F). Immunostaining of the cleaved caspase 3 demonstrated that the apoptotic index of epithelial cells was increased by 24-fold in *Pb-Csf1* mice (WT: 0.020 ± 0.0044% and PBC: 0.48 ± 0.11%) (Fig. 2G).

To determine how Csf1 overexpression causes the formation of PIN lesions, we examined where its receptor Csf1R was expressed in the prostate using a *Csf1R-GFP* reporter mouse line. Immunohistochemical analysis shows that GFP is exclusively expressed in the periglandular spaces (Supplementary Fig. 2C), indicating that prostate epithelial cells do not express Csf1R. Flow cytometric analysis further reveals that all GFP positive cells were Lin(CD45/CD31/Ter119)$^{+}$ positive cells, indicating that prostate epithelial and stromal cells did not express a detectable level of Csf1R either. This conclusion was confirmed by a *Csf1R-iCre;R26-LSL-eYFP* bigenic reporter model (Supplementary Fig. 2D). These results support that *Csf1* transgene expression induces PIN lesions indirectly through effects on immune cells.

RNA-seq analysis reveals inflammation-induced molecular changes in prostate epithelial cells.

To investigate how Csf1-mediated changes in the tissue microenvironment impacts prostate epithelial biology, we performed RNA-seq analyses on FACS isolated Lin^{-}CD24^{+}CD49f^{low} luminal epithelial cells (Fig. 3A) from 16-week-old *Pb-Csf1* and control wildtype mice. We identified 1324 genes that were differentially expressed by at least 2-fold between the two groups (Fig. 3B). As shown in Fig. 3C, gene set enrichment analysis (GSEA) showed that NF-κB signaling, P53 targets, senescence, epithelial stem/progenitor features, epithelial-to-mesenchymal transition (EMT), Il6-STAT3 signaling, and angiogenesis were upregulated, whereas RB1 targets, telomere maintenance, and unfolded protein response were downregulated in the *Pb-Csf1* group. These analyses not only corroborate an activation of the inflammatory signaling in the epithelial cells but also suggest downstream molecular mechanisms through which PIN lesions were induced in the *Pb-Csf1* model. We reason that human prostate cancer patients with high *CSF-1* expression display similar transcriptional alterations identified in the *Pb-Csf-1* model. We downloaded the expression data from TCGA PRAD study (31), and defined 43/290 (15%) cases with *CSF1* overexpression. *CSF1* overexpressed cases showed higher macrophage M2 cells compared to wild type cases (Fig. 3D), which is like the change in the anterior prostate of the *Pb-Csf-1* model. Given the

profound differences between mouse models and human patients, interspecies comparisons are difficult, and the baseline expectation is for there to be profound differences. Strikingly, gene set enrichment analysis (GSEA) showed the similar signaling pathways between human cases and mouse data (Fig. 3E), supporting the overall relevance of the mouse Csf1 model to the human disease. Overall, these results demonstrated that the transcriptional changes in the prostate epithelial cells of the *Pb-Csf1* model recapitulated those of human prostate cancer samples with higher *CSF-1* expression.

It should be mentioned that our analysis also revealed some differences such as the androgen response and the E2F targets. These differences may result from the nature of the comparison. The mouse data compares luminal epithelial cells from *Pb-Csf1* and control wildtype mouse, while the human data is a comparison across a population of prostate cancers from bulk sequencing. Additionally, although the "AR response" showed up in the GSEA analysis, the enrichment was not very significant.

To corroborate the increased gene signatures reflecting progenitor activity and EMT in the luminal cells in the *Pb-Csf1* model, we performed qRT-PCR analyses of key representative genes associated with progenitor identity and EMT using FACS-isolated luminal cells. Data shown in Figs. 4A and 4B confirmed that six EMT-associated genes and five stem cell-associated genes were all expressed at a higher level in the luminal cells of *Pb-Csf1* mice than those of WT mice. The increased progenitor activity is further supported by the observation that the organoid-forming unit of the VP luminal cells of *Pb-Csf1* mice was 13-fold higher than that of WT VP luminal cells (3.9 ± 0.44% versus 0.30 ± 0.0095%) (Fig. 4C) and that the organoid size was also 1.7-fold larger (181.4 ± 11.50 versus 108.1 ± 4.701 μm) (Fig. 4D). The induction of EMT was also further supported by immunostaining showing the expression of vimentin in prostatic epithelial cells of *Pb-Csf1* mice (white arrows, Fig. 4E). Immunostaining also showed phosphorylation of RB (Fig. 4F) and STAT3 (Fig. 4G) in the prostate of *Pb-Csf1* mice, supporting a decreased RB activity and an increased Il6-STAT3 activity.

Alleviating p53-mediated senescence promotes initiation of PIN lesions but does not result in progress to adenocarcinoma.

The GSEA analysis suggested an increased senescence in the *Pb-Csf1* model. Fig. 5A shows that the percentage of phosphorylated H2A.X positive epithelial cells in the *Pb-Csf1* mice is 5-fold higher than that in the control mice (WT: 0.26 ± 0.051% and *Pb-Csf1*: 1.37 ± 0.20%), which was further confirmed by a Western blot analysis (Fig. 5B). Prostate tissues of 1-year-old *Pb-Csf1* mice also showed a stronger activity of senescence-associated β-galactosidase (Fig. 5C).

To determine whether p53-mediated senescence restricted initiation and progression of PIN lesions in the *Pb-Csf1* model, we disrupted *p53* specifically in the prostate epithelial cells in this model by breeding it with the *Pb-Cre* and *P53* conditional knockout mice to generate the *Pb-Csf1;Pb-Cre;P53*$^{fl/fl}$ triple transgenic mice (hereafter referred to as *Pb-Csf1;p53*$^{Pb\text{-}Null}$). By 1.5 year of age, the prostatic weight of *p53*$^{Pb\text{-}Null}$ mice (105.2 ± 10.18 mg) was 1.7-fold of that of the control (66.68 ± 4.04 mg) and *Pb-Csf1* (63.41 ± 1.74 mg) mice (Fig. 5D). In contrast, the weight of *Pb-Csf1;p53*$^{Pb\text{-}Null}$ mice (175.2 ± 12.48 mg) was 2.8-fold of that

of *Pb-Csf1* mice. Disrupting epithelial p53 attenuated senescence as demonstrated by the reduced activity of senescence-associated β-galactosidase (Fig. 5E). Epithelial knockout of p53 alone occasionally led to the formation of smaller PIN II lesions with nuclear atypia in AP (Fig. 5F) but not in other lobes. Formation of PIN lesions in *Pb-Csf1;p53*$^{Pb\text{-}Null}$ mice significantly increased in AP but not in VP (Fig. 5F). The more pronounced nuclear pleomorphism with prominent nucleoli and the loss of cell polarity was consistent with PIN III. No evidence for invasive carcinoma was observed. P53 deletion further increased the percentage of CD45$^+$ leukocytes in AP but not VP (Supplementary Fig. 3A). The macrophage polarity was not affected in VP but the percentage of M2 macrophage was increased by 22.4% in AP (Supplementary Fig. 3A). Immunostaining of lineage markers showed that there was no obvious changes in epithelial cell lineage composition in the PIN lesions in *Pb-Csf1;p53*$^{Pb\text{-}Null}$ mice, except that Nkx3.1 was downregulated while vimentin was upregulated (Supplementary Fig. 3B). Ablating p53 significantly increased proliferating index of prostate epithelial cells as determined by immunostaining of Ki67 (Fig. 5G). Collectively, these results demonstrate that although loss of p53 can alleviate senescence and promote initiation of precancerous lesions, it is insufficient to progress PIN lesions to adenocarcinoma.

Il6/Gp130 signaling but not Il1 signaling plays a major role in Csf1-induced PIN formation.

Gp130 and IL1R are the receptors for Il-6 and Il-1, respectively. To determine whether Il6- and Il1-mediated signaling are necessary for the formation of PIN lesions in the *Pb-Csf1* mice, we generated the *Pb-Csf1;Pb-Cre;Gp130*$^{fl/fl}$ triple transgenic mice and *Pb-Csf1;IL1R*^{Null} mice (hereafter referred to as *Pb-Csf1;Gp130*$^{Pb\text{-}Null}$ and *Pb-Csf1;Il1R*^{Null} mice, respectively). We showed previously that eliminating Il1 signaling did not disrupt prostate homeostasis (26). Disrupting Il1 signaling in *Pb-Csf1* mice neither affected the formation of PIN lesions nor the degree of the PIN lesions. (Supplementary Figs. 4A and 4B). Interestingly, the percentages of CD45$^+$ leukocyte increased and macrophage polarity shifted towards M1 in AP of *Pb-Csf1;Il1R*^{Null} mice, whereas no obvious change was noted in VP (Supplementary Fig. 4C)

Eliminating epithelial *Gp130* alone did not affect prostate epithelial structure and lineage composition (*Gp130*$^{Pb\text{-}Null}$ mice in Fig. 6A) but substantially blocked the formation of PIN lesions in VP of 1-year-old *Pb-Csf1* mice. H&E staining showed that the ratio of glands with abnormal structure was significantly decreased in VP of *Pb-Csf1;Gp130*$^{Pb\text{-}Null}$ mice (15.69 ± 12.36%) (Figs. 6A and 6B). Fig. 6C and Supplementary Fig. 5 show that the percentage of Ki67$^+$ proliferating cells is significantly decreased upon ablation of *Gp130* (3.18 ±0.92% in *Pb-Csf1* mice vs. 0.49 ± 0.13% in *Pb-Csf1;Gp130*$^{Pb\text{-}Null}$ mice). The percentage of CD45$^+$ leukocyte and macrophage polarity in the prostate of *Pb-Csf1;Gp130*$^{Pb\text{-}Null}$ mice was mostly similar to those of *Pb-Csf1* mice, except for a minor decrease of CD45$^+$ cells in AP of *Pb-Csf1;Gp130*$^{Pb\text{-}Null}$ mice (Fig. 6D). These results demonstrate that Il6, but not Il1, plays a dominant role in the formation of the PIN lesions in VP of *Pb-Csf1* mice (Supplementary Fig. 5B).

Prostate inflammation alters AR transcriptome.

Inflammation has been shown to suppress the expression of AR and the biogenesis of dihydrotestosterone (10, 21, 32-34). Therefore, we sought to investigate whether the androgen signaling was affected in the *Pb-Csf1* model. QRT-PCR analysis shows that the expression of *Ar* and its several downstream target genes *Nkx3.1*, *Pbsn*, *Azgp1*, and *Msmb* were all downregulated in the FACS isolated luminal cells from *Pb-Csf1* mice compared to control mice (Fig. 7A). In Fig. 2C, immunostaining also shows that the expression levels of Ar and Nkx3.1 were decreased in inflamed areas in the *Pb-Csf1* model. This was further corroborated by the Western blot analysis of Ar and Nkx3.1 using FACS isolated luminal cells from the two groups (Fig. 7B).

To investigate whether inflammation affects the Ar binding at a genome scale, we performed AR ChIP-seq analysis using prostate tissues of *Pb-Csf1* and wildtype mice. The ChIP-seq analysis identified 30287 and 28555 ENCODE blacklist-filtered peaks in the WT and *Pb-Csf1* groups that were significantly enriched above the genomic ("input") control, respectively (Fig. 7C). Motif searches relied on existing database entries matched the ChIP-Seq data to the androgen responding element (ARE) (Fig. 7D), which corroborated a successful AR ChIP assay. There was no significant difference in AR binding intensity between the two groups at the global level (Fig. 7E) but by using differential peak calling we identified 2666 and 1066 peaks that were differentially bound by AR in the WT and *Pb-Csf1* groups, respectively (Fig. 7F). The respective 30287 and 28555 peaks identified in the WT and *Pb-Csf1* groups were distributed in various genomic foci including introns, exons, proximal promoter and UTRs, and intergenic regions (Fig. 7G, left). The distribution of the *Pb-Csf1* specific peaks was like that of the total peaks in each of the two groups (Fig. 7G, lower right). In sharp contrast, almost 90% of WT specific peaks exclusively resided in the intron and distal intergenic regions (Fig. 7G, upper right). The differentially bound peaks in the WT and *Pb-Csf1* groups fell in the region of 1325 and 1157 genes, respectively (Supplementary Table 2). Collectively, these results indicate that although there was no widespread change in global AR transcriptional activity in the *Pb-Csf1* model, binding of AR in a significant number of genes is altered.

To gain insight into how the AR binding at those 2482 genes was altered, we performed *de novo* motif search in their proximal promoter regions. The binding motifs of glucocorticoid response elements (GRE), forkhead box protein (FoxA1 and FoxI1), homeobox protein (Hoxd13 and Hoxc13), Sox4/5, and Arid3b/5a are enriched in the AR-bound genes in the WT group, whereas ZFX, AP-1, and Rbpj are identified as top motifs enriched in the specific AR-bound genes in the *Pb-Csf1* group (Supplementary Fig. 6). Of note, AP-1 is a critical mediator of inflammation and has been shown to serve as a co-factor with AR in macrophages (35). This supports that inflammatory signaling may regulate AR transcriptional activity via AP-1 in the *Pb-Csf1* model.

We further compared the RNA-seq and ChIP-Seq analyses to identify genes that were not only differentially expressed ($p<0.05$, t-test on log2-transformed data) by at least 1.3-fold between the WT and *Pb-Csf1* groups but also differentially bound by AR between the two groups (Supplementary Table 3). We identified 287 WT specific AR-bound genes with differential expression, among which 201 genes are expressed more than 1.3-fold in WT

over *Pb-Csf1* (such as *Prlr*) and 86 genes expressed at less than 1.3-fold (such as *Zeb1*, *Nfkb1*, *Ncoa3*) in the WT group. Conversely, 344 specific AR-bound genes were identified in the *Pb-Csf1* group among which 253 were upregulated in *Pb-Csf1* (*Ccnd2*, *Tacstd2*, *Sox4*, *Lcn2*, *Vangl1*, *Col4a1/2* etc.) and 91 downregulated. Fig. 7H shows 5 examples. These genes were likely positively or negatively regulated by AR directly, some of which have been reported previously such as *Prlr* and *Zeb1* (36, 37).

Discussion

Prostate inflammation and prostate cancer initiation and progression.

Our study shows that an increased level of versatile inflammatory cytokines and chemokines can only induce the formation of low-grade PIN lesions. Inflammation induces p53-mediated senescence, but attenuating senescence by ablating p53 is not sufficient to promote the formation of high-grade PIN lesions or adenocarcinoma. This indicates that senescence does not limit progression of the low-grade PIN lesions. Many inflammatory factors including Il1α/β, Cxcl1/2, and TNFα etc. were upregulated in the prostate of *Pb-Csf1* mice. However, the overall phenotype of the *Pb-Csf1* model is not significantly severer than those reported in the other mouse models overexpressing individual inflammatory cytokines (21-23). This indicates that the signaling mediated by different inflammatory signaling may not synergize substantially, which is not unexpected as these signaling often overlaps or converges. However, we showed that the Il6 signaling plays a dominant role in the formation of PIN lesions in the *Pb-Csf1* model. This is consistent with previous studies showing that the Il6/STAT3 signaling plays an essential role in the growth and progression of several tumor models (38-41). Collectively, our study supports that asymptomatic chronic prostate inflammation is a risk factor for prostate cancer but is not sufficient to transform prostate epithelial cells *de novo*. Interestingly, ectopic expression of Csf1 in mammary gland epithelial cells resulted in mammary gland tumors (28). It is possible that the expression level of the *Csf1* transgene is higher in that model or crosstalk between inflammation and hormonal signaling impacts disease progression in female-specific organs differently.

We demonstrated that the genes associated with EMT and stem cells are upregulated in the prostate luminal cells of *Pb-Csf1* mice. We also noticed that several AR-regulated secretory proteins were downregulated. These changes support an acinar-to-ductal transition of the luminal cells, which is analogous to how pancreatic epithelial cells respond to tissue injury (42). Epigenetic regulation associated with injury-induced chromatin states may play a critical role in the transition. Increased EMT and stem cell features are also consistent with the observations that inflammation promotes invasion and metastasis in many cancers including the prostate cancer. Expression of the macrophage inhibitory cytokine-1 (MIC-1) in myeloid cells in the TRAMP prostate cancer model resulted in smaller prostate tumor size but marked increase of distal metastases (43). Recently, it has been appreciated that oncogenic signaling can instigate tumor cell-intrinsic inflammatory signaling that remodels tumor microenvironment and promotes tumor progression. For examples, activation of β-Catenin in melanoma cells downregulates Ccl4, which prevents dendritic cell recruitment and T cell exclusion from the tumor microenvironment (44). Myc activation causes production of CCL9 and IL23 from lung adenoma epithelial cells, which

recruit macrophage and exclude NK, T and B cells (45). It is tempting to hypothesize that breeding the *Pb-Csf1* model with the mouse models for prostate cancer may promote tumor metastasis.

We showed that Csf1R is exclusively expressed in the immune cells in normal mouse prostate. Therefore, the epithelial phenotype displayed in the *Pb-Csf1* model is induced by Csf1 indirectly via the immune cells. However, Csf1R was also shown expressed by breast and prostate cancer cells and its expression level in cancer cells is correlated with poor prognosis (46, 47). Csf1R is also reported to be expressed by cancer associated fibroblast cells (CAFs). Csf1 downregulates granulocyte-specific chemokine expression in CAFs, and limits granulocyte recruitment to tumors (48). Therefore, Csf1 can also promote tumor growth and progression in a tumor cell-autonomous or CAF cell-mediated manner.

Crosstalk between AR and inflammatory signaling.

Androgen signaling plays a critical role in prostate cancer initiation and progression. A mutual regulation between AR and inflammatory signaling has been revealed. Androgen signaling suppresses inflammation. For example, androgen supplementation suppresses metabolic syndrome-associated prostate inflammation in a rabbit model (49) whereas anti-androgen therapies for benign prostate hyperplasia and prostate cancer induce immune cell infiltration and increased production of pro-inflammatory cytokines (50-52). AR can mediate signaling in different cell lineages to suppress inflammation. We showed previously that ablating AR in the mouse prostate luminal cells upregulated cytokine production and resulted in an inflammatory prostate microenvironment (26). AR signaling in the immune cells including macrophage also mediates an immunosuppressive effect (53). There are also studies showing AR as an enhancer for M2 macrophage polarization in the prostate and lung (35, 54).

On the other hand, inflammatory signaling has also been shown to regulates AR signaling in different ways. In *in vitro* studies, NF-κB and STAT3 can stimulate AR signaling (55, 56); TNFα regulates AR transcriptome (29); IL1β signaling dismisses the N-CoR/HDAC complex and permits de-repression of AR target genes (11). In contrast, inflammatory signaling is mostly reported to suppress AR signaling *in vivo*. In human prostate specimens, inflammation is inversely correlated with the expression of *SRD5A2*, a critical enzyme to produce dihydrotestosterone (57). Hypogonadism was associated with a fivefold increased risk of intraprostatic inflammation (34). AR is downregulated in bacterial infection-induced prostate inflammation models (10, 21, 32, 33), although it is not significantly altered in the prostate-specific Il6 overexpression model (23). Our study showed that AR and several AR-regulated genes are downregulated in the *Pb-Csf1* model. In addition, we showed that binding of AR in a significant number of genes is altered in the *Pb-Csf1* prostate luminal cells. Interestingly, our study showed that AP-1 is a motif enriched in the specific AR-bound genes in the *Pb-Csf1* luminal cells. It has been reported that AR binds DNA using the AP-1 complex as a co-factor in fibroblast (58) and macrophages (35). It is possible that utilization of AP-1 as an AR cofactor is a feature associated with inflammation and EMT. Collectively, most *in vivo* evidence supports that AR signaling suppresses inflammation whereas inflammation negatively impacts AR signaling. This double negative feedback loop

forms a vicious cycle, through which a chronic prostate inflammation can be initiated and sustained either by an ageing-associated progressive decline in serum testosterone levels, tissue damage, or incidental infection etc.

Methods

Mice

The *Tg(Csf1r-EGFP)1Hume/J*, *Tg(Csf1r-icre)1Jwp/J*, *Trp53*^{tm1Brn}*/J*, *Il1r1*^{tm1Imx}*/J*, *Gt(ROSA)26Sor*$^{tm1(EYFP)Cos/J}$, *Csf1R-GFP*, *Csf1R-iCre,* and *R26-LSL-eYFP* mice were purchased from The Jackson Laboratory (Bar Harbor, ME). *Gp130*$^{fl/fl}$ mice were from Dr. Rodger McEver at the University of Oklahoma Health Sciences Center. The *ARR2PB-Cre* transgenic mice were from Dr. Fen Wang at the Institute of Bioscience and Technology, Texas A&M Health Science Center. Mice were genotyped by polymerase chain reaction using mouse genomic DNA from tail biopsy specimens. The sequences of genotyping primers are listed in Supplementary Table 4. PCR products were separated electophoretically on 1% agarose gels and visualized via ethidium bromide under UV light. All the mice used in this study received humane care in compliance with the principles stated in the Guide for the Care and Use of Laboratory Animals, NIH Publication, 1996 edition, and the protocols were approved by the Institutional Animal Care Committee at the Baylor College of Medicine and the University of Washington.

Generation of Csf1 overexpressing transgenic mouse.

The full-length mouse *Csf1* cDNA, a generous gift from Dr. Richard Stanley, was PCR amplified using PrimeSTAR Max Premix (2X) (Takara, Mountain View, CA), cloned into the pGEM-T easy vector (Promega, Madison, WI), and sequenced to confirm that all the coding sequence is correct. The primers used for amplification are forward: 5’-AAAGCTAGCGCCGCCACCATGACCGCGCGGGGCGCCGC-3’ and reverse: 5’-TTTGAGCTCTATACTGGCAGTTCCACCTG −3’. The cDNA was released using *NheI* and *SacI* and was subsequently ligated into the ARR2PB-intron-BGHpA vector (gift from Dr. Fen Wang) using the Takara Ligation Kit (Takara, Mountain View, CA), resulting in the final m*Csf-1* transgenic vector. The fragment containing the composite probasin promoter, intron, *Csf1* and *BGH-pA* was released by *SalI* and *NotI*, gel purified, and used for pronuclear microinjection at the transgenic facility at the Baylor College of Medicine.

Mice carrying the *ARR2PB-Csf1* cassette were identified by PCR analysis of tail-derived genomic DNA using primers amplifying a 405bp fragment within the mCsf-1 cDNA. The primers were: sense primer: 5’-CCTGTGTCCGAACTTTCCAT-3’ and antisense primer: 5’-TTGGTTGCTCTGTTGACTCG-3’. The primers also generate a 1546bp fragment from the endogenous *Csf1* genomic sequence, which was used as an internal control for successful PCR reaction from DNA to exclude false negative. 11 out of 32 pups delivered by foster mothers tested positive for the transgene. Three lines failed germline transfer.

RNA isolation, quantitative RT–PCR, and RT2 Profiler™ PCR Array

Total RNA was extracted using Nucleospin RNA XS plus Kit (Macherey-Nagel, Bethlehem, PA). RNA was reverse transcribed to cDNA using iScript™ Reverse Transcription Supermix

(Bio-Rad, Hercules, CA). QRT-PCR was performed using SYBR Green system (Bio-Rad) and detected on a StepOne plus Real-Time PCR system (Applied Biosystems, Foster City, CA). Primers for target genes are listed in Supplementary Table 5. Analysis of mouse cytokines and chemokines was performed on RT^2 Profiler™ PCR Array Mouse inflammatory cytokines and receptors plates following the manufacturer's instruction (Qiagen, Valencia, CA).

Preparation of dissociated mouse prostate single cells and flow cytometry

Prostate tissues were dissociated into single cells according to the procedure described previously (59). Briefly, mouse prostate tissues were incubated in DMEM/Collagenase/Hyaluronidase/FBS (STEMCELL technologies, Vancouver, Canada) for 3 hours at 37°C, followed by a one hour-incubation in 0.25% Trypsin-EDTA (Invitrogen, Carlsbad, CA) on ice. Thereafter, mouse prostate tissues were pelleted, resuspended in Dispase (Invitrogen, Carlsbad, CA, 5 mg/mL) and DNase I (Roche Applied Science, Indianapolis, IN, 1 mg/mL), and pipetted vigorously to dissociate cell clumps. Dissociated cells were then passed through 70 μm cell strainers (BD Biosciences, San Jose, CA) to obtain single cells. Dissociated single mouse prostate cells were incubated with florescence conjugated antibodies on ice for 30 minutes. After washing with 10% FBS-containing DMEM, FACS analyses and sorting were performed using the BD LSR II, and Aria II (BD Biosciences, San Jose, CA). Gating was set up using fluorescence minus one. Antibodies for FACS analysis and sorting are listed in Supplementary Table 6.

Senescence array

Senescence associated β-galactosidase staining was performed using the Senescence β-Galactosidase Staining Kit (Cat#9860, Cell Signaling Technologies, Danvers, MA) on frozen sections from OCT (optimal cutting temperature compound)-embedded prostate tissues according to the manufacturer's instruction. Tissues were stained for 4 hours at 37 °C in dark.

Histology, Masson's trichrome staining and Immunostaining

Prostate tissues were fixed by 10% buffered formalin and paraffin embedded. H&E, Masson's trichrome and immunofluorescence staining were performed using standard protocols on 5-μm paraffin sections. Masson's trichrome stain was performed according to the manufacture's instruction (HT15-1KT, Sigma- Aldrich, St. Louis, MO). For immunostaining, sections were deparaffinized, and antigen retrieval was performed by steam heating in Tris-EDTA Buffer (10mM Tris Base, 1mM EDTA Solution, 0.05% Tween 20, pH 9.0) for 10 min in steamer. Slides were incubated with 5% normal goat serum (Vector Labs, Burlingame, CA) and with primary antibodies diluted in 3% normal goat serum overnight at 4°C. Information for primary antibodies is listed in Supplementary Table 7. Slides were then incubated with secondary antibodies. Sections were counterstained with hematoxylin or NucBlue™ Fixed Cell ReadyProbes™ Reagent (Thermo Fisher). Immunohistological staining was imaged using Leica DM4B fluorescent microscope or LeicaSP8 confocal microscope (Leica Microsystems, Wetzlar, Germany). All representative images were quantified by the Image J software.

RNA-seq

NucleoSpin RNA XS Kit (Macherey-Nagel, Bethlehem, PA) was used to purify RNAs from FACS-isolated mouse luminal cells from WT and *Pb-Csf1*. Reverse transcriptions were performed using SMART SeqTM v4 UltraTM Low Input RNA Kit for Sequencing (Clontech Laboratories, Mountain View, CA). CDNA libraries were prepared using Nextera XT DNA Library Preparation Kit (Illumina, San Diego, CA) and sequenced using HiSeq 2500 sequencer. Sequenced reads in FASTQ files were mapped to mm10 whole genome using Tophat2, and Fragments Per Kilobase of transcript per Million mapped reads (FPKM) were calculated using Cufflinks. FPKM values were quantile normalized. Differential expression between comparison groups was defined using two-sided t-test on log2-transformed data. Gene Set Enrichment Analysis (GSEA) was carried out using Signal2Noise metric and weighted scoring. Data have been deposited at GEO (accession number pending).

Murine prostate organoid assay

FACS-isolated basal and luminal cells from WT and *Pb-Csf1* mice were cultured in Corning® Matrigel® Basement Membrane Matrix (Corning, Tewksbury, MA) with advanced DMEM/F12 supplemented with B27 (Life technologies, Grand Island, NY), 10 mM HEPES, glutamax (Life technologies, Grand Island, NY), penicillin/streptomycin, and the following growth factors: EGF 50 ng/ml (Peprotech, Rocky Hill, NJ), 500 ng/ml recombinant R-spondin1 (Peprotech, Rocky Hill, NJ), 100 ng/ml recombinant Noggin (Peprotech, Rocky Hill, NJ), 200 nM of TGF-β/Alk inhibitor A83-01 (Tocris, Ellisville, MO), and 10 μm Y-27632 (Tocris, Ellisville, MO). Dihydrotestosterone (DHT) (Sigma, St. Louis, MO) was added to a final concentration of 1 nM.

Western blot, Enzyme-linked immunosorbent assay, and cytokine antibody array

Prostate tissues and cells were lysed in RIPA buffer (20 mM Tris-HCl, pH 7.5, 150 mM NaCl, 1 mM Na_2EDTA, 1 mM EGTA, 1% NP-40, 1% sodium deoxycholate, 2.5 mM sodium pyrophosphate, 1 mM β-glycerophosphate, 1 mM Na_3VO_4) with protease inhibitors and phosphatase inhibitors (GeneDEPOT, Houston, TX) using Tissuelyser LT (Qiagen, Valencia, CA). Protein concentrations were determined by a Bradford Assay kit (BioRad, Hercules, CA). Protein was separated by 8% or 12% SDS/PAGE and transferred onto a PVDF membrane (Amersham Biosciences, Arlington Heights, IL). Membrane was blocked in 5% skim milk, and subsequently incubated with primary antibodies listed in Supplementary Table 7 at 4°C overnight followed by incubation with peroxidase-conjugated goat anti-mouse IgG or goat anti-rabbit IgG (Jackson ImmunoResearch, Inc., West Grove, PA), and developed with Pierce ECL reagent (Thermal Scientific, Rockford, IL). Mouse M-CSF Quantikine ELISA kit (Cat# MMC00, R&D systems, Minneapolis, MN) was used to determine Csf1 level in prostate lysates according to the manufacturer's instruction. Proteome Profiler Mouse Cytokine Array Kit (ARY006, R&D System, Inc,, Minneapolis, MN) was used to determine cytokine expression in total prostate lysates according to the manufacturer's instruction.

The expression data of human localized prostate cancer cases were downloaded from TCGA PRAD study (PMID: 26544944), and overexpressed *CSF1* cases were defined as cases with

CSF1 expression more than one standard deviation based on the expression z-score relative to diploid samples from cBioPortal (https://www.cbioportal.org/). CIBERSORT (PMID: 25822800) was used to quantify the abundance of immune cells in TCGA PRAD cases. Differentially expressed genes were identified between overexpressed *CSF1* and wild type cases and enriched signaling pathways were detected via gene set enrichment analysis (GSEA) (PMID: 16199517).

ChIP-seq

For AR ChIP-seq, fresh prostate tissues from 12-week-old *Pb-Csf1* and control WT C57Bl/6 male mice were snap-frozen in liquid nitrogen and shipped to Active Motif for FactorPath ChIP-seq as described previously (60) using anti-AR antibody (sc-816; Santa Cruz Biotechnology). Illumina sequencing libraries were prepared from the ChIP and Input DNAs by the standard consecutive enzymatic steps of end-polishing, dA-addition, and adaptor ligation. After a final PCR amplification step, the resulting DNA libraries were quantified and sequenced on Illumina's NextSeq 500 (75 nt reads, single end). Reads were aligned to the mouse genome (mm10) using the BWA algorithm (default settings). Duplicate reads were removed, and only uniquely mapped reads (mapping quality >= 25) were used for further analysis. Alignments were extended *in silico* at their 3'-ends to a length of 200 bp, which is the average genomic fragment length in the size-selected library and assigned to 32-nt bins along the genome. The resulting histograms (genomic "signal maps") were stored in bigWig files. Peak locations were determined using the MACS algorithm (v1.4.2) with a cutoff of p-value = 1e-7 and Input DNA data as "control" file. For differential MACS peak calling, the WT and *Pb-Csf1* data files were used as "treatment" and "control" file, respectively, and vice versa, using the same p-value cutoff. Signal maps and peak locations were used as input data to Active Motifs proprietary analysis program, which creates Excel tables containing detailed information on sample comparison, peak metrics, peak locations, and gene annotations.

Statistics

All experiments were performed using 3-18 mice in independent experiments. Data are presented as mean ± SD or mean ± SEM. Student's t test was used to determine significance between groups. All p values reported were two-sided unless otherwise noted. For all statistical tests, the 0.05 level of confidence was accepted for statistical significance.

Supplementary Material

Refer to Web version on PubMed Central for supplementary material.

Acknowledgements

We thank Dr. Fen Wang for the ARR2PB-Cre mice, Dr. Rodger McEver for the $Gp130^{fl/fl}$ mice, and Dr. Richard Stanley for the mouse *Csf-1* cDNA. This work is supported by R01CA190378, R01DK092202 and R01DK107436 (L.X.).

Source of support:

NCI, NIDDK

References

1. De Marzo AM, Platz EA, Sutcliffe S, Xu J, Gronberg H, Drake CG, et al. Inflammation in prostate carcinogenesis. Nature reviews Cancer. 2007;7(4):256–69. Epub 2007/03/27. [PubMed: 17384581]
2. Mantovani A, Allavena P, Sica A, Balkwill F. Cancer-related inflammation. Nature. 2008;454(7203):436–44. Epub 2008/07/25. [PubMed: 18650914]
3. Kazma R, Mefford JA, Cheng I, Plummer SJ, Levin AM, Rybicki BA, et al. Association of the innate immunity and inflammation pathway with advanced prostate cancer risk. PLoS One. 2012;7(12):e51680. Epub 2012/12/29. [PubMed: 23272139]
4. Platz EA, Kulac I, Barber JR, Drake CG, Joshu CE, Nelson WG, et al. A Prospective Study of Chronic Inflammation in Benign Prostate Tissue and Risk of Prostate Cancer: Linked PCPT and SELECT Cohorts. Cancer epidemiology, biomarkers & prevention : a publication of the American Association for Cancer Research, cosponsored by the American Society of Preventive Oncology. 2017;26(10):1549–57. Epub 2017/07/30.
5. Gurel B, Lucia MS, Thompson IM Jr., , Goodman PJ, Tangen CM, Kristal AR, et al. Chronic inflammation in benign prostate tissue is associated with high-grade prostate cancer in the placebo arm of the prostate cancer prevention trial. Cancer epidemiology, biomarkers & prevention : a publication of the American Association for Cancer Research, cosponsored by the American Society of Preventive Oncology. 2014;23(5):847–56. Epub 2014/04/22.
6. Dennis LK, Lynch CF, Torner JC. Epidemiologic association between prostatitis and prostate cancer. Urology. 2002;60(1):78–83. Epub 2002/07/09.
7. De Marzo AM, Marchi VL, Epstein JI, Nelson WG. Proliferative inflammatory atrophy of the prostate: implications for prostatic carcinogenesis. Am J Pathol. 1999;155(6):1985–92. Epub 1999/12/14. [PubMed: 10595928]
8. Endo Y, Marusawa H, Kinoshita K, Morisawa T, Sakurai T, Okazaki IM, et al. Expression of activation-induced cytidine deaminase in human hepatocytes via NF-kappaB signaling. Oncogene. 2007;26(38):5587–95. Epub 2007/04/04. [PubMed: 17404578]
9. Hmadcha A, Bedoya FJ, Sobrino F, Pintado E. Methylation-dependent gene silencing induced by interleukin 1beta via nitric oxide production. The Journal of experimental medicine. 1999;190(11):1595–604. Epub 1999/12/10. [PubMed: 10587350]
10. Debelec-Butuner B, Alapinar C, Varisli L, Erbaykent-Tepedelen B, Hamid SM, Gonen-Korkmaz C, et al. Inflammation-mediated abrogation of androgen signaling: an in vitro model of prostate cell inflammation. Molecular carcinogenesis. 2014;53(2):85–97. Epub 2012/08/23. [PubMed: 22911881]
11. Zhu P, Baek SH, Bourk EM, Ohgi KA, Garcia-Bassets I, Sanjo H, et al. Macrophage/cancer cell interactions mediate hormone resistance by a nuclear receptor derepression pathway. Cell. 2006;124(3):615–29. Epub 2006/02/14. [PubMed: 16469706]
12. Grivennikov SI, Greten FR, Karin M. Immunity, inflammation, and cancer. Cell. 2010;140(6):883–99. Epub 2010/03/23. [PubMed: 20303878]
13. Kwon OJ, Zhang B, Zhang L, Xin L. High fat diet promotes prostatic basal-to-luminal differentiation and accelerates initiation of prostate epithelial hyperplasia originated from basal cells. Stem cell research. 2016;16(3):682–91. Epub 2016/04/24. [PubMed: 27107344]
14. Kwon OJ, Zhang L, Ittmann MM, Xin L. Prostatic inflammation enhances basal-to-luminal differentiation and accelerates initiation of prostate cancer with a basal cell origin. Proc Natl Acad Sci U S A. 2014;111(5):E592–600. Epub 2013/12/25. [PubMed: 24367088]
15. Jin RJ, Lho Y, Connelly L, Wang Y, Yu X, Saint Jean L, et al. The nuclear factor-kappaB pathway controls the progression of prostate cancer to androgen-independent growth. Cancer Res. 2008;68(16):6762–9. Epub 2008/08/15. [PubMed: 18701501]
16. Luo JL, Tan W, Ricono JM, Korchynskyi O, Zhang M, Gonias SL, et al. Nuclear cytokine-activated IKKalpha controls prostate cancer metastasis by repressing Maspin. Nature. 2007;446(7136):690–4. Epub 2007/03/23. [PubMed: 17377533]
17. Birbach A, Eisenbarth D, Kozakowski N, Ladenhauf E, Schmidt-Supprian M, Schmid JA. Persistent inflammation leads to proliferative neoplasia and loss of smooth muscle cells in a prostate tumor model. Neoplasia. 2011;13(8):692–703. Epub 2011/08/19. [PubMed: 21847361]

18. Elkahwaji JE, Zhong W, Hopkins WJ, Bushman W. Chronic bacterial infection and inflammation incite reactive hyperplasia in a mouse model of chronic prostatitis. Prostate. 2007;67(1):14–21. Epub 2006/11/01. [PubMed: 17075821]
19. Fong L, Ruegg CL, Brockstedt D, Engleman EG, Laus R. Induction of tissue-specific autoimmune prostatitis with prostatic acid phosphatase immunization: implications for immunotherapy of prostate cancer. J Immunol. 1997;159(7):3113–7. Epub 1997/10/08. [PubMed: 9317107]
20. Haverkamp JM, Charbonneau B, Crist SA, Meyerholz DK, Cohen MB, Snyder PW, et al. An inducible model of abacterial prostatitis induces antigen specific inflammatory and proliferative changes in the murine prostate. Prostate. 2011;71(11):1139–50. Epub 2011/06/10. [PubMed: 21656824]
21. Khalili M, Mutton LN, Gurel B, Hicks JL, De Marzo AM, Bieberich CJ. Loss of Nkx3.1 expression in bacterial prostatitis: a potential link between inflammation and neoplasia. Am J Pathol. 2010;176(5):2259–68. Epub 2010/04/07. [PubMed: 20363913]
22. Barron DA, Strand DW, Ressler SJ, Dang TD, Hayward SW, Yang F, et al. TGF-beta1 induces an age-dependent inflammation of nerve ganglia and fibroplasia in the prostate gland stroma of a novel transgenic mouse. PLoS One. 2010;5(10):e13751. Epub 2010/11/10. [PubMed: 21060787]
23. Liu G, Zhang J, Frey L, Gang X, Wu K, Liu Q, et al. Prostate-specific IL-6 transgene autonomously induce prostate neoplasm through amplifying inflammation in the prostate and peri-prostatic adipose tissue. Journal of hematology & oncology. 2017;10(1):14. Epub 2017/01/13. [PubMed: 28077171]
24. Wang X, Lin WJ, Izumi K, Jiang Q, Lai KP, Xu D, et al. Increased infiltrated macrophages in benign prostatic hyperplasia (BPH): role of stromal androgen receptor in macrophage-induced prostate stromal cell proliferation. The Journal of biological chemistry. 2012;287(22):18376–85. Epub 2012/04/05. [PubMed: 22474290]
25. Lissbrant IF, Stattin P, Wikstrom P, Damber JE, Egevad L, Bergh A. Tumor associated macrophages in human prostate cancer: relation to clinicopathological variables and survival. International journal of oncology. 2000;17(3):445–51. Epub 2000/08/12. [PubMed: 10938382]
26. Zhang B, Kwon OJ, Henry G, Malewska A, Wei X, Zhang L, et al. Non-Cell-Autonomous Regulation of Prostate Epithelial Homeostasis by Androgen Receptor. Molecular cell. 2016;63(6):976–89. Epub 2016/09/07. [PubMed: 27594448]
27. Stanley ER, Chitu V. CSF-1 receptor signaling in myeloid cells. Cold Spring Harbor perspectives in biology. 2014;6(6). Epub 2014/06/04.
28. Kirma N, Luthra R, Jones J, Liu YG, Nair HB, Mandava U, et al. Overexpression of the colony-stimulating factor (CSF-1) and/or its receptor c-fms in mammary glands of transgenic mice results in hyperplasia and tumor formation. Cancer Res. 2004;64(12):4162–70. Epub 2004/06/19. [PubMed: 15205327]
29. Malinen M, Niskanen EA, Kaikkonen MU, Palvimo JJ. Crosstalk between androgen and pro-inflammatory signaling remodels androgen receptor and NF-kappaB cistrome to reprogram the prostate cancer cell transcriptome. Nucleic acids research. 2017;45(2):619–30. Epub 2016/09/28. [PubMed: 27672034]
30. Park JH, Walls JE, Galvez JJ, Kim M, Abate-Shen C, Shen MM, et al. Prostatic intraepithelial neoplasia in genetically engineered mice. Am J Pathol. 2002;161(2):727–35. Epub 2002/08/07. [PubMed: 12163397]
31. The Molecular Taxonomy of Primary Prostate Cancer. Cell. 2015;163(4):1011–25. Epub 2015/11/07. [PubMed: 26544944]
32. Simons BW, Durham NM, Bruno TC, Grosso JF, Schaeffer AJ, Ross AE, et al. A Human Prostatic Bacterial Isolate Alters the Prostatic Microenvironment and Accelerates Prostate Cancer Progression. The Journal of pathology. 2014. Epub 2014/10/29.
33. Shinohara DB, Vaghasia AM, Yu SH, Mak TN, Bruggemann H, Nelson WG, et al. A mouse model of chronic prostatic inflammation using a human prostate cancer-derived isolate of Propionibacterium acnes. Prostate. 2013;73(9):1007–15. Epub 2013/02/08. [PubMed: 23389852]
34. Vignozzi L, Cellai I, Santi R, Lombardelli L, Morelli A, Comeglio P, et al. Antiinflammatory effect of androgen receptor activation in human benign prostatic hyperplasia cells. The Journal of endocrinology. 2012;214(1):31–43. Epub 2012/05/09. [PubMed: 22562653]

35. Cioni B, Zaalberg A, van Beijnum JR, Melis MHM, van Burgsteden J, Muraro MJ, et al. Androgen receptor signalling in macrophages promotes TREM-1-mediated prostate cancer cell line migration and invasion. Nature communications. 2020;11(1):4498. Epub 2020/09/11.
36. Ormandy CJ, Clarke CL, Kelly PA, Sutherland RL. Androgen regulation of prolactin-receptor gene expression in MCF-7 and MDA-MB-453 human breast cancer cells. International journal of cancer Journal international du cancer. 1992;50(5):777–82. Epub 1992/03/12. [PubMed: 1544711]
37. Graham TR, Yacoub R, Taliaferro-Smith L, Osunkoya AO, Odero-Marah VA, Liu T, et al. Reciprocal regulation of ZEB1 and AR in triple negative breast cancer cells. Breast cancer research and treatment. 2010;123(1):139–47. Epub 2009/11/19. [PubMed: 19921427]
38. Grivennikov S, Karin E, Terzic J, Mucida D, Yu GY, Vallabhapurapu S, et al. IL-6 and Stat3 are required for survival of intestinal epithelial cells and development of colitis-associated cancer. Cancer Cell. 2009;15(2):103–13. Epub 2009/02/03. [PubMed: 19185845]
39. Bollrath J, Phesse TJ, von Burstin VA, Putoczki T, Bennecke M, Bateman T, et al. gp130-mediated Stat3 activation in enterocytes regulates cell survival and cell-cycle progression during colitis-associated tumorigenesis. Cancer Cell. 2009;15(2):91–102. Epub 2009/02/03. [PubMed: 19185844]
40. Naugler WE, Sakurai T, Kim S, Maeda S, Kim K, Elsharkawy AM, et al. Gender disparity in liver cancer due to sex differences in MyD88-dependent IL-6 production. Science. 2007;317(5834):121–4. Epub 2007/07/07. [PubMed: 17615358]
41. Chan KS, Sano S, Kiguchi K, Anders J, Komazawa N, Takeda J, et al. Disruption of Stat3 reveals a critical role in both the initiation and the promotion stages of epithelial carcinogenesis. The Journal of clinical investigation. 2004;114(5):720–8. Epub 2004/09/03. [PubMed: 15343391]
42. Strobel O, Dor Y, Alsina J, Stirman A, Lauwers G, Trainor A, et al. In vivo lineage tracing defines the role of acinar-to-ductal transdifferentiation in inflammatory ductal metaplasia. Gastroenterology. 2007;133(6):1999–2009. Epub 2007/12/07. [PubMed: 18054571]
43. Husaini Y, Qiu MR, Lockwood GP, Luo XW, Shang P, Kuffner T, et al. Macrophage inhibitory cytokine-1 (MIC-1/GDF15) slows cancer development but increases metastases in TRAMP prostate cancer prone mice. PLoS One. 2012;7(8):e43833. Epub 2012/09/07. [PubMed: 22952779]
44. Spranger S, Bao R, Gajewski TF. Melanoma-intrinsic beta-catenin signalling prevents anti-tumour immunity. Nature. 2015;523(7559):231–5. Epub 2015/05/15. [PubMed: 25970248]
45. Kortlever RM, Sodir NM, Wilson CH, Burkhart DL, Pellegrinet L, Brown Swigart L, et al. Myc Cooperates with Ras by Programming Inflammation and Immune Suppression. Cell. 2017;171(6):1301–15 e14. Epub 2017/12/02. [PubMed: 29195074]
46. Lin EY, Nguyen AV, Russell RG, Pollard JW. Colony-stimulating factor 1 promotes progression of mammary tumors to malignancy. The Journal of experimental medicine. 2001;193(6):727–40. Epub 2001/03/21. [PubMed: 11257139]
47. Ide H, Seligson DB, Memarzadeh S, Xin L, Horvath S, Dubey P, et al. Expression of colony-stimulating factor 1 receptor during prostate development and prostate cancer progression. Proc Natl Acad Sci U S A. 2002;99(22):14404–9. [PubMed: 12381783]
48. Kumar V, Donthireddy L, Marvel D, Condamine T, Wang F, Lavilla-Alonso S, et al. Cancer-Associated Fibroblasts Neutralize the Anti-tumor Effect of CSF1 Receptor Blockade by Inducing PMN-MDSC Infiltration of Tumors. Cancer Cell. 2017;32(5):654–68 e5. Epub 2017/11/15. [PubMed: 29136508]
49. Vignozzi L, Morelli A, Sarchielli E, Comeglio P, Filippi S, Cellai I, et al. Testosterone protects from metabolic syndrome-associated prostate inflammation: an experimental study in rabbit. The Journal of endocrinology. 2012;212(1):71–84. Epub 2011/10/20. [PubMed: 22010203]
50. Maggio M, Basaria S, Ceda GP, Ble A, Ling SM, Bandinelli S, et al. The relationship between testosterone and molecular markers of inflammation in older men. Journal of endocrinological investigation. 2005;28(11 Suppl Proceedings):116–9. Epub 2006/06/09. [PubMed: 16760639]
51. Maggio M, Blackford A, Taub D, Carducci M, Ble A, Metter EJ, et al. Circulating inflammatory cytokine expression in men with prostate cancer undergoing androgen deprivation therapy. Journal of andrology. 2006;27(6):725–8. Epub 2006/06/16. [PubMed: 16775253]
52. Sorrentino C, Musiani P, Pompa P, Cipollone G, Di Carlo E. Androgen deprivation boosts prostatic infiltration of cytotoxic and regulatory T lymphocytes and has no effect on disease-free survival

in prostate cancer patients. Clin Cancer Res. 2011;17(6):1571–81. Epub 2010/12/17. [PubMed: 21159885]

53. Traish A, Bolanos J, Nair S, Saad F, Morgentaler A. Do Androgens Modulate the Pathophysiological Pathways of Inflammation? Appraising the Contemporary Evidence. Journal of clinical medicine. 2018;7(12). Epub 2018/12/19.
54. Becerra-Diaz M, Strickland AB, Keselman A, Heller NM. Androgen and Androgen Receptor as Enhancers of M2 Macrophage Polarization in Allergic Lung Inflammation. J Immunol. 2018;201(10):2923–33. Epub 2018/10/12. [PubMed: 30305328]
55. Chen T, Wang LH, Farrar WL. Interleukin 6 activates androgen receptor-mediated gene expression through a signal transducer and activator of transcription 3-dependent pathway in LNCaP prostate cancer cells. Cancer Res. 2000;60(8):2132–5. Epub 2000/04/29. [PubMed: 10786674]
56. Zhang L, Altuwaijri S, Deng F, Chen L, Lal P, Bhanot UK, et al. NF-kappaB regulates androgen receptor expression and prostate cancer growth. Am J Pathol. 2009;175(2):489–99. Epub 2009/07/25. [PubMed: 19628766]
57. Wang Z, Hu L, Salari K, Bechis SK, Ge R, Wu S, et al. Androgenic to oestrogenic switch in the human adult prostate gland is regulated by epigenetic silencing of steroid 5alpha-reductase 2. The Journal of pathology. 2017;243(4):457–67. Epub 2017/09/25. [PubMed: 28940538]
58. Leach DA, Panagopoulos V, Nash C, Bevan C, Thomson AA, Selth LA, et al. Cell-lineage specificity and role of AP-1 in the prostate fibroblast androgen receptor cistrome. Molecular and cellular endocrinology. 2017;439:261–72. Epub 2016/09/17. [PubMed: 27634452]
59. Valdez JM, Zhang L, Su Q, Dakhova O, Zhang Y, Shahi P, et al. Notch and TGFbeta form a reciprocal positive regulatory loop that suppresses murine prostate basal stem/progenitor cell activity. Cell stem cell. 2012;11(5):676–88. Epub 2012/11/06. [PubMed: 23122291]
60. Hewitt SC, Li L, Grimm SA, Chen Y, Liu L, Li Y, et al. Research resource: whole-genome estrogen receptor alpha binding in mouse uterine tissue revealed by ChIP-seq. Mol Endocrinol. 2012;26(5):887–98. Epub 2012/03/27. [PubMed: 22446102]

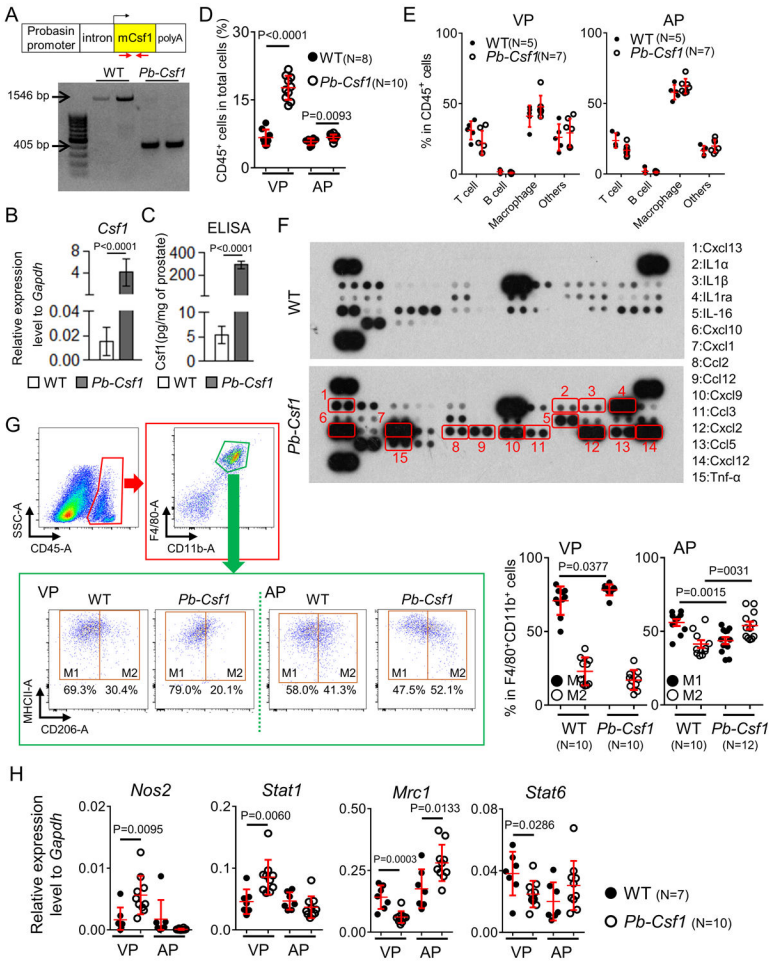

Figure 1. Csf1 overexpression recruits immune cells and alters polarization of macrophage in mouse prostate.

(A) Schematic illustration of *Pb-Csf1* transgenic model and genotyping strategy. (B-C) Bar graphs show means ± SD of expression of *Csf1* gene by qRT-PCR (B) and Csf1 protein by ELISA (C) in mouse prostates. N=3. WT: wild type. (D) Dot plot shows means ± SD of percentage of $CD45^+$ cells in ventral (VP) and anterior (AP) prostates of 1-yr-old WT and *Pb-Csf1* mice. (E) Dot plots show means ± SD of percentage of T, B, and macrophage in $CD45^+$ cells of VP (left) and AP (right) of 1-yr-old WT and *Pb-Csf1* mice. (F) Cytokine array using prostate lysate of 4-mo-old WT and *Pb-Csf1* mice. (G) FACS plot shows surface marker expression of macrophage. Dot plots show means ± SD of percentage of pro-inflammatory $MHCII^+CD206^-$ (M1) and anti-inflammatory $MHCII^+CD206^+$ (M2) macrophages in $F4/80^+CD11b^+$ cells of VP (left) and AP (right) of 1-year-old WT and *Pb-Csf1* mice. (H) Dot plots show means ± SD of expression of 4 macrophage polarization markers in $F4/80^+CD11b^+$ cells of VP and AP of 1-yr-old WT and *Pb-Csf1* mice.

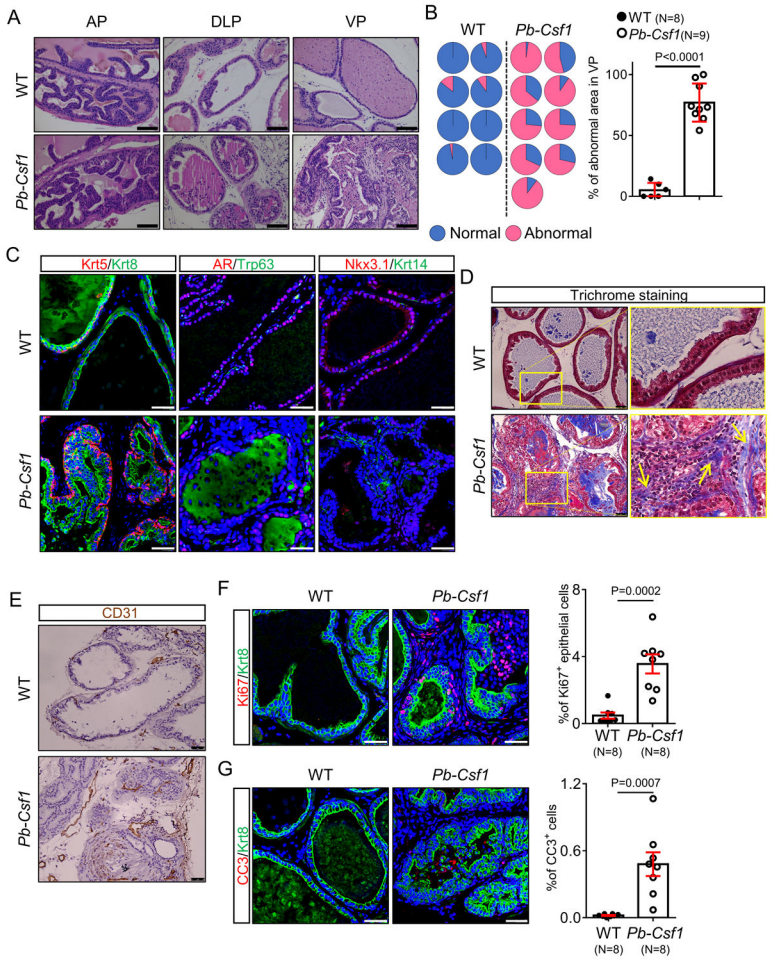

Figure 2. Csf1 overexpression causes prostatic intraepithelial neoplasia.

(A) H&E staining of anterior (AP), dorsolateral (DLP), and ventral (VP) prostates of 1-yr-old WT and *Pb-Csf1* mice. Yellow arrows point to immune cell infiltration in VP. Scale bars=100 μm. (B) Pie charts show percentage of VP region with abnormal histology in individual 1-yr-old WT and *Pb-Csf1* mice. Bar graph shows means ± SD of percentage of area with abnormal histology. (C) Co-immunostaining of Krt5/Krt8, AR/Trp63, and Nkx3.1/Krt14 in VP of 1-yr-old WT and *Pb-Csf1* mice. Scale bars=50 μm. (D-E) Masson's trichrome staining (D) and immunostaining of CD31 (E) in VP of 1-yr-old WT and *Pb-Csf1* mice. Scale bars=50 μm. Yellow arrows point to collagen deposition. (F-G) Co-immunostaining of Ki67/Krt8 (F) and Cleaved caspase-3 (CC3)/Krt8 (G) in VP of 1-yr-old WT and *Pb-Csf1* mice. Scale bars=50 μm. Dot graphs show means ± SD of percentage of $Ki67^+$ epithelial cells (F) and $CC3^+$ cells (G). Results are from 11-17 representative images per mouse.

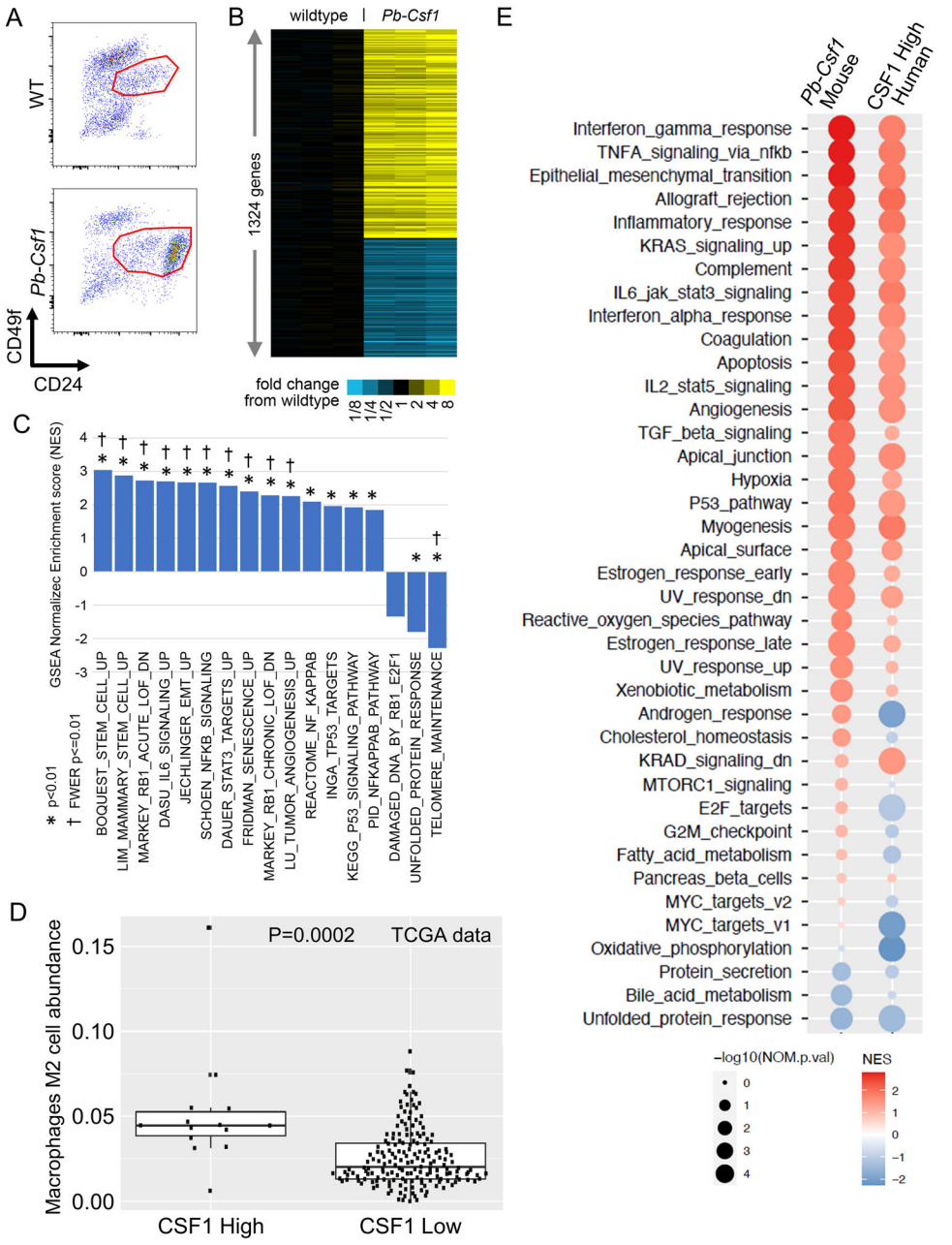

Figure 3. RNA-seq reveals inflammation-induced molecular changes in prostate luminal cells.

(A) FACS plots of Lin^{-}CD24^{+}CD49f^{low} luminal cells (marked by red polygons) in 4-mo-old WT and *Pb-Csf1* (lower) mice. (B) Heatmap of top differentially expressed genes using RNA-seq analysis, at p<0.01 (t-test on log2-transformed data) and fold change>2. (C) Bar graph shows normalized enrichment scores (NES) by GSEA of positively (+) and negatively (−) enriched gene sets in *Pb-Csf1* luminal cells as compared to WT. FWER, family-Wise Error Rate. (D) Arbitrary index of macrophage M2 cell abundance derived from TCGA cases via CIBERSORT in prostate cancer patients with relatively high and low CSF1 expression. (E) Dot plot show comparison of GSEA analyses for Pb-Csf1 and human prostate cancer patients with high CSF1 expression.

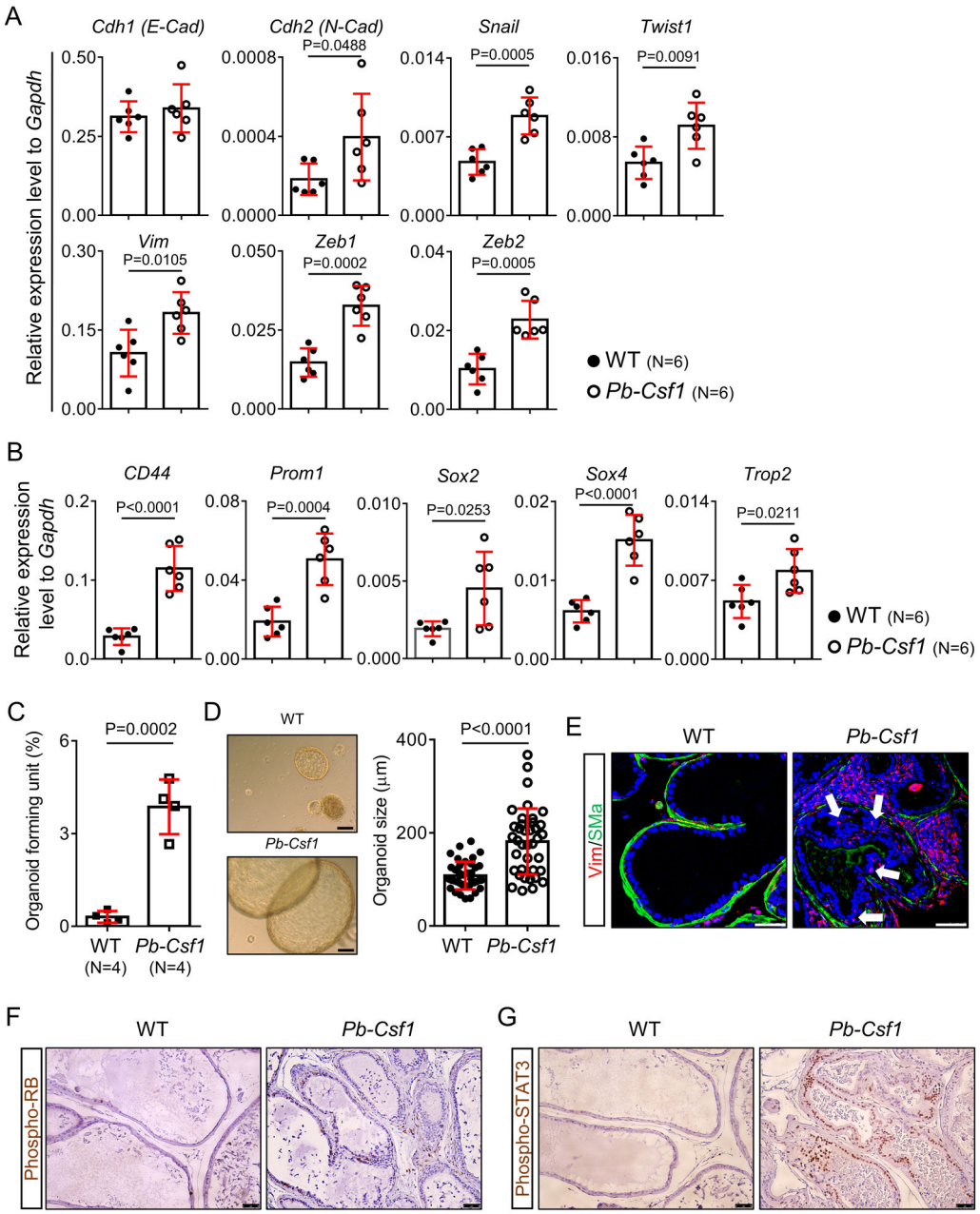

Figure 4. Csf1 overexpression increases EMT and progenitor activity-related gene signatures.

(A-B) Bar graphs show means ± SD of expression of 7 epithelial-to-mesenchymal transition (EMT)-related genes (A) and 5 Stem/progenitor activity-related genes (B) by qRT-PCR in luminal cells of 1-yr-old WT and *Pb-Csf1* mice. (C) Bar graph shows means ± SD of organoid forming unit of $Lin^{-}CD24^{+}CD49^{low}$ luminal cells of ventral prostate (VP) of 1-yr-old WT and *Pb-Csf1* mice (N=4) (D) Transilluminating images show organoids derived from each group. Scale bars=50 μm. Bar graph shows means ± SD of organoid size (N=39-109 from 4 independent experiments). (E) Co-immunostaining of vimentin (Vim)/ smooth muscle actin (SMa) in ventral prostate of 1-yr-old WT and *Pb-Csf1* mice. White arrows point to Vim^{+} cells in epithelium. Scale bars=50 μm. (F-G) Immunostaining of

phospho-retinoblastoma (RB) (D) and phospho-STAT3 (E) in ventral prostate of 1-yr-old WT and *Pb-Csf1* mice. Scale bars=50 μm.

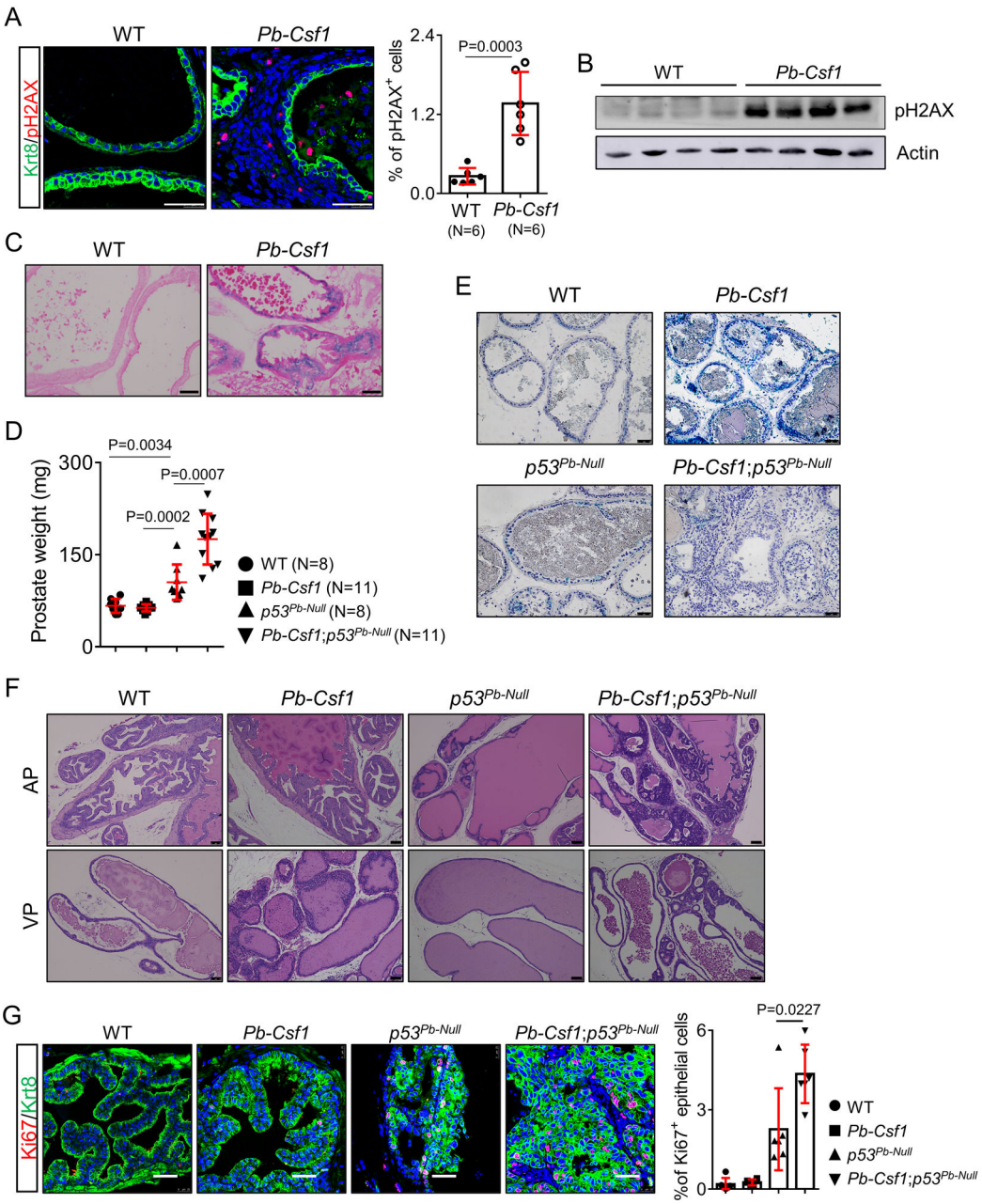

Figure 5. Attenuating p53-mediated senescence promotes initiation of PIN lesions.

(A) Co-immunostaining of Krt8/phospho-Histone H2A.X (Ser139) (pH2AX) in ventral prostate of 1-yr-old WT and *Pb-Csf1* mice. Scale bars=50 μm. Dot plot shows means ± SD of percentage of $pH2AX^+$ cells. Results are from 18-24 representative images per mouse. (B) Western blot of pH2AX and β-actin in FACS-sorted luminal cells from 1-yr-old WT and *Pb-Csf1* mice. (C) Senescence-associated β-galactosidase assay in ventral prostate of 1-yr-old WT and *Pb-Csf1* mice. Blue color indicates senescence. Scale bars=50 μm. (D) Dot plot shows mean ± SD of prostate weight of 1.5-yr-old mice. (E) Senescence-associated β-galactosidase assay in ventral prostate of 1.5-yr-old mice. Scale bars=25 μm. (F-G) H&E staining in anterior (AP) and ventral (VP) prostate (F) and co-immunostaining of Ki67/

Krt8 (G) of AP of 1.5-yr-old mice. Scale bars=50 μm. Bar graph shows means ± SD of percentage of $Ki67^+$ cells in AP (N=6, results are from 13-15 representative images per mouse).

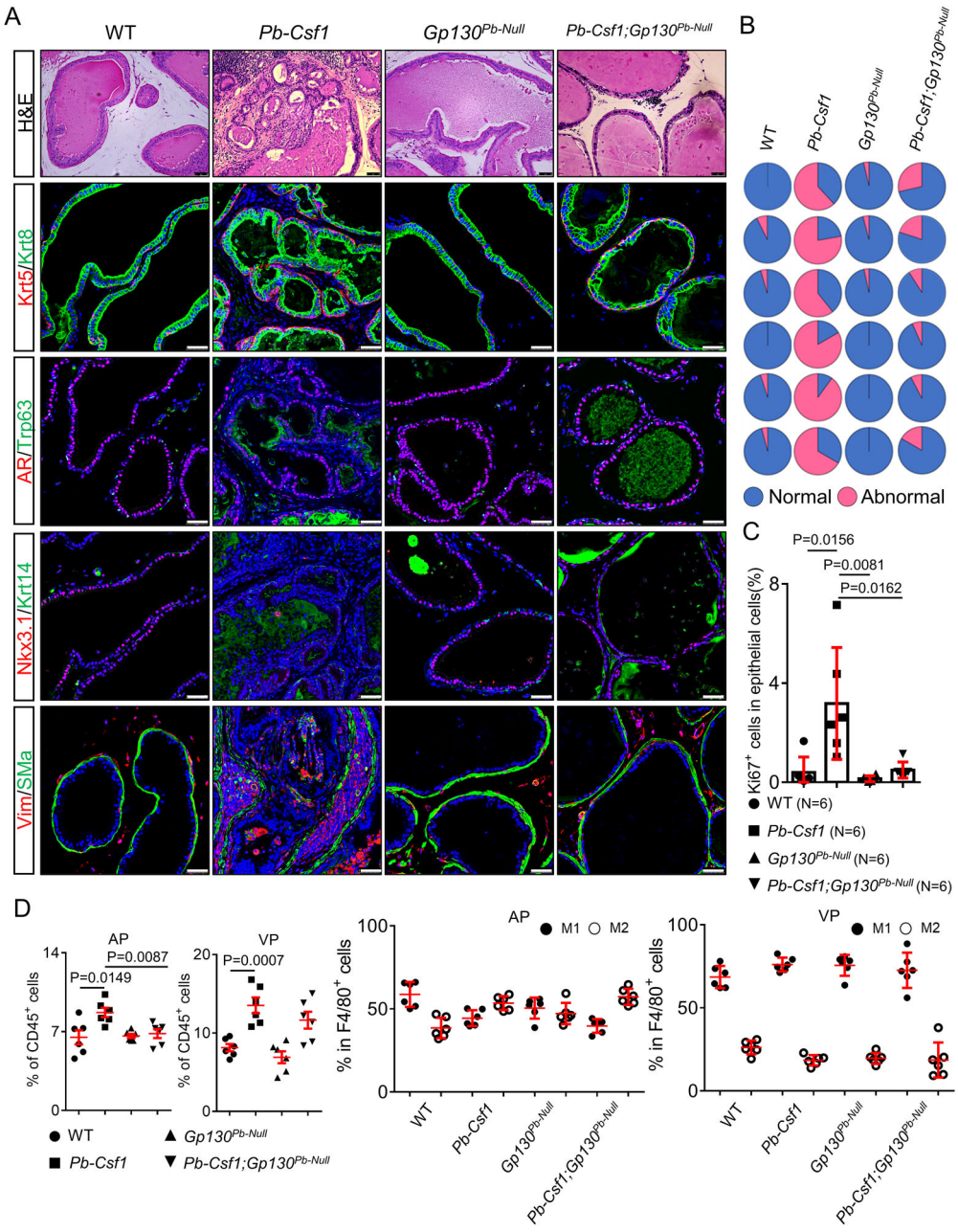

Figure 6. Il6-Gp130 signaling is necessary for formation of Csf1-induced prostate intraepithelial neoplasia.

(A) H&E staining and co-immunostaining of Krt5/Krt8, AR/Trp63, Nkx3.1/Krt14, and Vim/SMa in ventral prostate of 1-yr-old mice. Scale bars=50 μm. (B) Pie charts show percentage of area in ventral prostate with abnormal histology in individual mice (N=6). (C) Bar graph shows means ± SD of percentage of $Ki67^+$ cells in ventral prostate of 1-yr-old mice. Results are from 17-22 representative images per mouse. (D) Dot plots show percentages of $CD45^+$ leukocytes, M1 and M2 macrophages in anterior prostate (AP) and ventral (VP) prostate of 1-yr-old mice (N=6) by flow cytometry analysis.

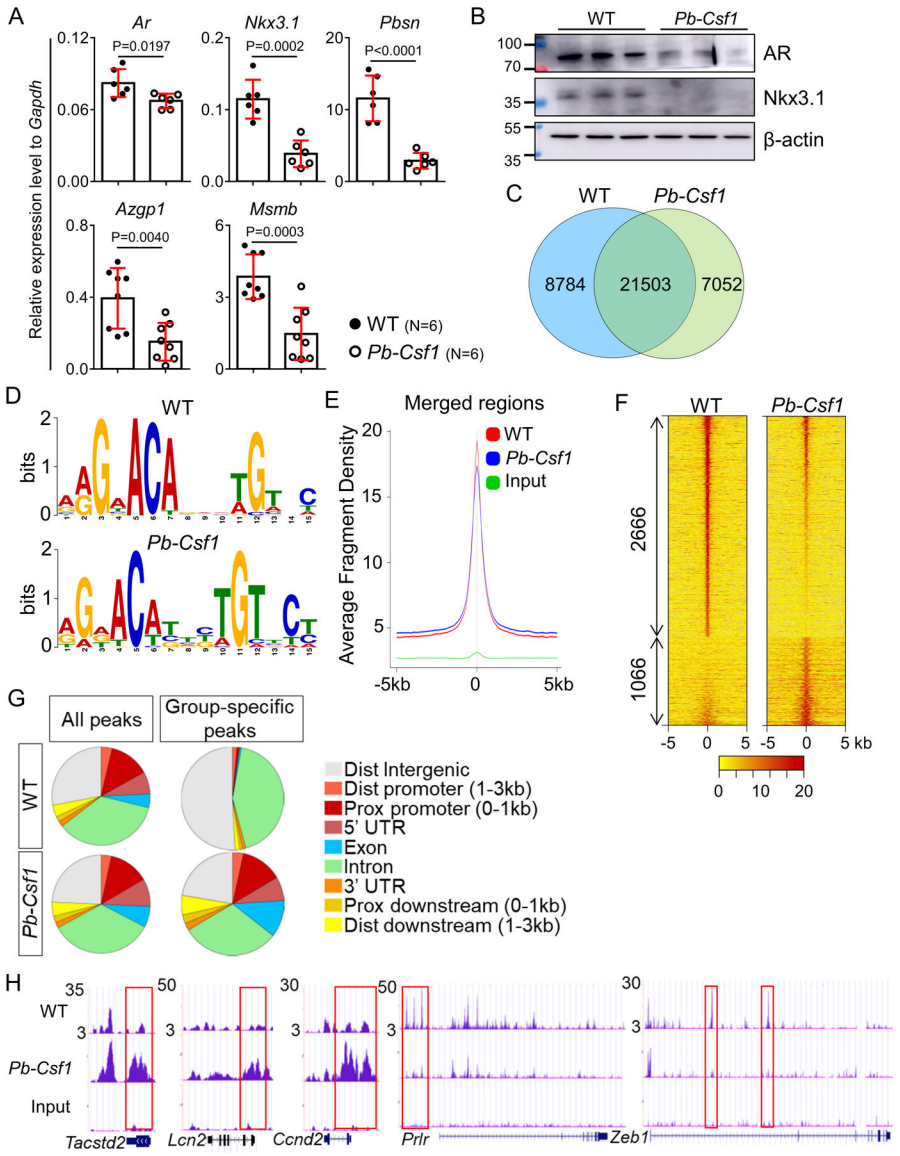

Figure 7. Prostate inflammation alters AR transcriptome.

(A) Dot plots show means ± SD of expression of *Ar* and 4 AR target genes by qRT-PCR in FACS-isolated luminal cells of 1-yr-old WT and *Pb-Csf1* mice. (B) Western blot of AR, Nkx3.1, and β-actin in FACS-sorted luminal cells from 1-yr-old WT and *Pb-Csf1* mice. (C) VENN diagram of standard analysis showing regions where a peak was called in WT, *Pb-Csf1*, and both groups. (D): Binding motifs identified *de novo* from peaks in WT and *Pb-Csf1* groups by TOMTOM/MEME. The height of nucleotide represents the probability at the respective position. (E) Average density plot of tag distributions across peak regions. (F) Heatmaps show 2666 and 1066 differentially AR-bound sites in WT and *Pb-Csf1* groups, respectively. Color bar shows ChIP intensity. (G) Pie charts show genome distribution of peaks. (H) UCSC genome browser screenshots show differential binding of AR in 5 representative genes. Red boxes highlight differentially bound regions.